VPS VIBRATIONS IN PHYSICAL SYSTEMS

DOI: 10.21008/j.0860-6897.2021.1.09
Vibrations in Physical Systems, 32(1):2021109, 2021

Influence of the Elastic Cavity Walls on Cavity Flow Noise

Paweł ŁOJEK[1], Ireneusz CZAJKA[1], Andrzej GOŁAŚ[1], Katarzyna SUDER-DĘBSKA[1]

Corresponding author: Paweł ŁOJEK, email: lojek@agh.edu.pl

[1] AGH University of Science and Technology, Department of Power Systems and Environmental Protection Facilities, 30 Mickiewicza Av., 30-059 Kraków, Poland

Abstract In this study, computational fluid dynamics and computational aeroacoustics methods were used to investigate the influence of the elastic cavity walls on the noise generated by the flow over rectangular cavity. Two cases were considered and compared, one with rigid cavity walls, and one with elastic walls. In the latter case, the movement of the walls were solved by finite element modelling and coupled with CFD simulations. The noise generated by the flow over cavity was computed using Ffowcs Williams & Hawkings acoustic analogy. The increase of the sound pressure level for elastic walls case at frequency range of 1 kHz to 10 kHz is observed, compared to the rigid walls case.

Keywords: FSI, Detached Eddy Simulations, Acoustic analogy, cavity noise

1. Introduction

Turbulent flow through structural discontinuities (diffusers, grilles, nozzles, etc) is one of the causes of noise generation in air ducts (others being turbomachinery noise) [1, 2]. In this study, we analyse the flow through such discontinuity, using the example of duct with rectangular cavity. Such flow has been studied extensively in e.g. [3, 4, 5, 6]. Nevertheless, we are focusing on this issue for two reasons: in most cases, the Mach number for the flows is greater than 0.8 – the analysed flows are transonic or supersonic, and because there are no aeroacoustical analyses taking flexible cavity walls into account. There are papers on the lid driven cavity flows with flexible walls, e.g. [7, 8], however, they focus on heat transfer and do not consider the phenomena that may occur in the ventilation duct, or noise induced by the flow. In [9] the cavity flow is analysed but focus of the study is again a heat transfer, moreover, in this case only a downstream wall was treated as elastic.

This paper investigates the fluid-structure interaction (FSI) between flow and cavity walls and its impact on the flow and noise generation.

2. Methods

2.1. Fluid modelling

Turbulent fluid motion inside the duct was solved with Finite Volume Method and OpenFOAM software [10]. The $k-\omega$ SST DES (Detached Eddy Simulation) [11] model was used to describe the fluid motion. This model uses Large Eddy Simulation (LES) equations in the separated region and uRANS (unsteady Reynolds Averaged Navier-Stokes) equations with $k-\omega$ SST turbulence model as closure equations.

The Navier-Stokes equations for incompressible Newtonian fluids are given by [12]:

$$\frac{\partial v_i}{\partial x_i} = 0, \tag{1}$$

$$\frac{\partial v_i}{\partial t} + v_j \frac{\partial v_i}{\partial x_j} = -\frac{1}{\rho}\frac{\partial p}{\partial x_i} + \nu \nabla^2 v_i \tag{2}$$

where: v_i – i-th component of velocity, p – pressure, ρ – density, $\nu = \mu/\rho$ – kinematic viscosity.

Depending on the method (LES/RANS) the equations are decomposed, by spatial filtering or by Reynolds averaging and solved with the Finite Volume Element (FVM) method.

2.2. Solid modelling

The structural part of the model was solved using CalculiX Finite Element software [13]. The motion of the body is described by general momentum equation:

$$[M]\{\ddot{U}\} + [K]\{U\} = \{F\} \tag{3}$$

where: $\{\ddot{U}\} = \{A\}$ – global acceleration vector, $\{U\}$ – global displacement vector, $[M]$ – global mass matrix, $[K]$ – global stiffness matrix, $\{F\}$ – global force vector.

The equation is discretized and solved with Finite Element Method. PreCICE allows only for linear element coupling, so 8-node brick element (C38D), general purpose and fully integrated element, was used for discretization of the cavity walls. The shape functions of this element are given by [14]:

$$\varphi = \frac{1}{8}(1 + \xi\xi_i)(1 + \eta\eta_i) \tag{4}$$

where: ξ_i, η_i, ζ_i – local coordinates of the ith point.

2.3. Fluid-structure interaction

PreCICE library [15] was used to couple fluid flow and solid displacement fields. Besides fluid-structure interaction, it allows conjugate heat transfer, structure-structure, and fluid-fluid coupling. The library also offers several methods for solving equations and for data mapping between different fields and meshes. In this study, we used serial explicit coupling scheme for solving interface equations and nearest-neighbour and nearest-projection methods for data mapping.

For FSI simulations, the displacement and force fields are exchanged between solvers after each time step. The forces exerted by the fluid on the cavity walls are boundary conditions for the structural simulations. The results of FEM simulations – displacement field, is transferred to the FVM flow model as mesh displacement [16].

2.4. Aeroacoustics

Acoustic analogies were used to compute noise generated by the flow in the vicinity of the cavity. Due to the presence of movable walls, the Ffowcs Williams-Hawkings (FW-H) acoustic analogy was used [17]. This analogy allows for description of the acoustic pressure radiated by turbulent flow in the presence of arbitrarily moving surfaces.

$$\frac{1}{c^2}\frac{\partial^2 p'}{\partial t^2} - \nabla^2 p' = \frac{\partial}{\partial t}\left[\rho_0 v_n \delta(f)\right] - \frac{\partial}{\partial x_i}\left[p n_i \delta(f)\right] + \frac{\partial^2}{\partial x_i \partial x_j}\left[H(f) T_{ij}\right] \tag{5}$$

where: p' – acoustic pressure, $f(x,t)$ – moving surface, c – speed of sound, $\delta(f)$ – Dirac's delta function, $H(f)$ – Heaviside function, $T_{ij} = \rho u_i u_j - \sigma_{ij} + (p' - c^2\rho')\delta_{ij}$ – Lighthill stress tensor.

The equation is solved and written as:

$$p'^{(x,t)} = p'_T(x,t) + p'_L(x,t) \tag{6}$$

$$p'_T(x,t) = \frac{1}{4\pi}\int_{f=0}\left[\frac{\rho_0(\dot{v}_n + v_{\dot{n}})}{1|1 - M_r|^2}\right]_{ret} \mathrm{d}S + \frac{1}{4\pi}\int_{f=0}\left[\frac{\rho_0 v_n (r\dot{M}_r + cM_r - cM^2)}{1|1 - M_r|^3}\right]_{ret} \mathrm{d}S \tag{7}$$

(8)

$$p'_L(x,t) = \frac{1}{4\pi c}\int_{f=0}\left[\frac{\dot{l}_r}{r|1 - M_r|^2}\right]_{ret} \mathrm{d}S + \frac{1}{4\pi c}\int_{f=0}\left[\frac{l_r - l_M}{r|1 - M_r|^2}\right]_{ret} \mathrm{d}S + \frac{1}{4\pi c}\int_{f=0}\left[\frac{l_r(r\dot{M}_r + cM_r - cM^2)}{r^2\,|1 - M_r|^3}\right]_{ret} \mathrm{d}S$$

This formulation of FW-H equation solution is known as Farassat 1A formulation [18,19] and allows for direct computation of acoustic pressure at observer's position. 1A formulation allows using permeable surfaces surrounding noise sources as source surfaces. However, in this study this feature of 1A formulation was not used, and cavity walls was used as source surface.

The analogy is implemented in OpenFOAM as in [20], or in *libAcoustics*, library for far-field noise computations [21].

3. Simulation setup

The rectangular duct with rectangular cavity was adapted as fluid flow model. It was shown in the Fig. 1 while its dimensions are described in Tab. 1, the depth of computational domain was 0.125 m. The computational mesh was created with cfMesh open-source library and consisted of 200 thousand cells. Mesh boundary layer allowed to achieve the y^+ value lesser than 1, required by the adapted model.

Tab. 1. Dimensions of the model

h	D	L	l_1	l_2
0.125	0.03	0.12	0.1	0.5

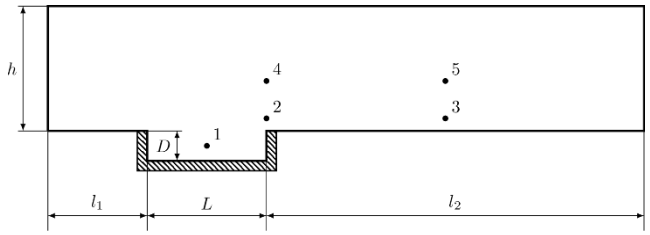

Fig. 1. Analyzed model of the cavity, location of the pressure probes.

3.1. Material parameters

The air at 20˚C was used as material for flow simulations. The density and kinematic viscosity of the air in such conditions are given by $\rho = 1.23$ kg/m^3 and $1.5 \cdot 10^{-5}$ m^2/s.

For structural simulations, the aluminium was used as material, with Young's modulus, Poisson's ratio and density given by $E = 70 \cdot 10^9$ Pa, $\nu = 0.33$ and $\rho = 2700$ kg/m^3. The choice of material was due to the fact that the ventilation ducts are often made of an aluminium sheet with such dimensions and parameters.

3.2. Initial and boundary conditions

The boundary conditions of fluid simulations were shown in tab. 2 The inlet was placed on the left side of the domain, outlet – on the right. Remaining boundaries of the domain were treated like walls. The cavity walls were flexible and able to move, based on displacements from FEM simulations, the rest (before and after the cavity and at the top) were rigid, also, cavity walls were marked as interface between simulations.

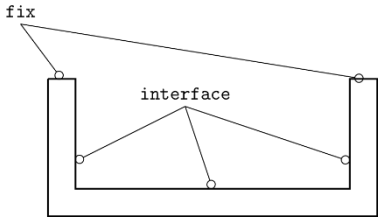

Fig. 2. Boundaries of finite element model (not in scale).

The boundary conditions imposed on cavity walls in structural simulations were shown in the fig. 2. At the *fix* boundary, all nodes were constrained with displacement and rotation in each direction fixed. The

boundary named *interface* acted as the interface between simulations. In addition, forces resulting from fluid flow simulations were applied to nodes at this boundary.

Tab. 2. Fluid simulations boundary conditions.

	Pressure p [Pa]	Velocity u [m/s]	Turbulent kinetic energy k [m²/s²]	Specific dissipation ratio ω [1/s]	Turbulent viscosity ν_t [m²/s]
Wall	$\frac{\partial p}{\partial x_n} = 0$	$u_i = 0$	$k = 0$	$\omega = 8 \cdot 10^6$	$\nu_t = 0$
Inlet	$\frac{\partial p}{\partial x_n} = 0$	$u_x = 15,$ $u_{y,z} = 0$	$k = 3.375$	$\omega = 2500$	calculated
Outlet	$p = 0$	$\frac{\partial u_i}{\partial x_n} = 0$	$\frac{\partial k}{\partial x_n} = 0$	$\frac{\partial \omega}{\partial x_n} = 0$	calculated

4. Results and discussion

This section presents the numerical results for pressure inside the duct, displacement of the cavity walls, and acoustic pressure computed with FW-H analogy (equations (6-8)) The results obtained for the case with flexible walls were compared with the results obtained for the case with rigid walls.

4.1. Flow field results

In this subsection, the flow field results obtained with OpenFOAM software are presented, both for velocity and pressure. Pressure data collected at selected probes were also analyzed by means of Fourier transform to obtain the frequency distribution. The pressure probe placement is shown in the Tab. 3. and in the Fig. 1. The probe 1 is located in the middle of the cavity and the remaining probes are placed at the downstream.

The pressure time values and their spectra inside the cavity, shown in the Fig. 3 and at the downstream edge (Fig. 4) are similar to each other, and this type of low frequency fluctuations and vortices are typical for flows over cavities [3, 6, 22].

Tab. 3. Pressure probes location.

#	x [m]	y [m]	z [m]
1	0.016	-0.15	0.0625
2	0.12	0.01	0.0625
3	0.5	0.01	0.0625
4	0.12	0.05	0.0625
5	0.05	0.05	0.0625

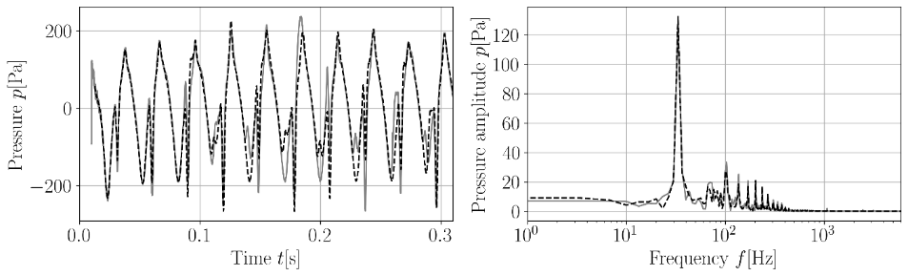

Fig. 3. Pressure values at probe 1 (—— - flexible walls, ----- - rigid walls).

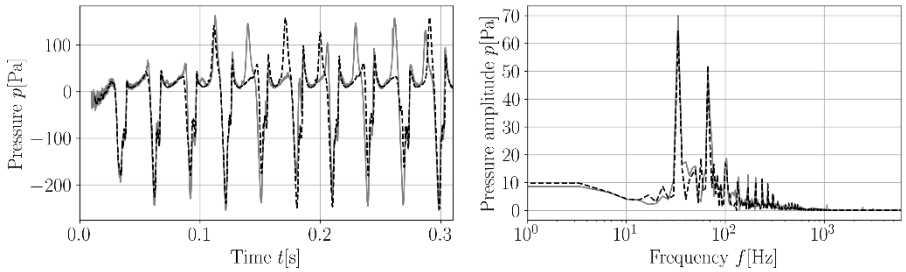

Fig. 4. Pressure values at probe 2 (——— - flexible walls, ----- - rigid walls).

However, for probes further away from the cavity, numbered 3, 4 and 5 (Figs 5-7), additional fluctuations of pressure can be noticed. They may have the cause in fluid-elastic cavity oscillations [22]. As it can be seen in the Fig. 9, if the deformation of the cavity walls is considered, the nature and frequency of resulting vortices changes compared to the rigid walls.

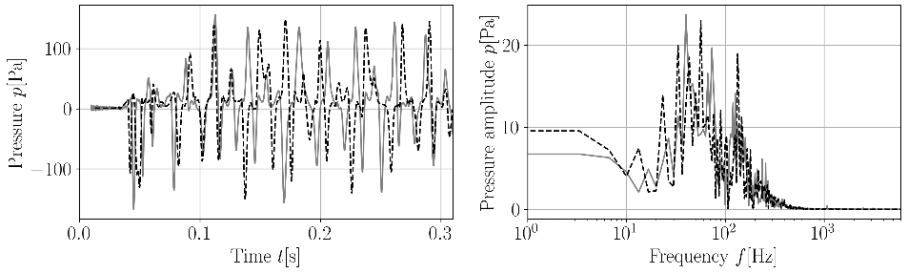

Fig. 5. Pressure values at probe 3 (——— - flexible walls, ----- - rigid walls).

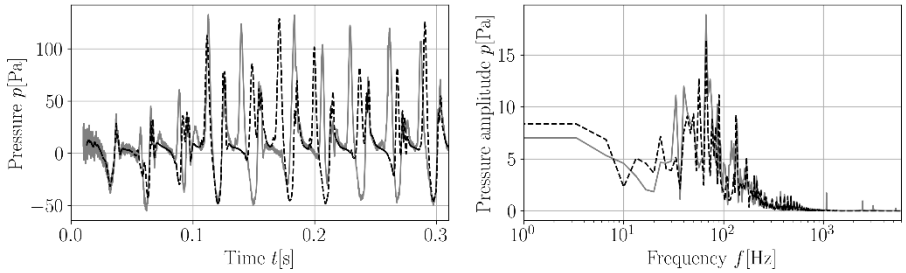

Fig. 6. Pressure values at probe 4 (——— - flexible walls, ----- - rigid walls).

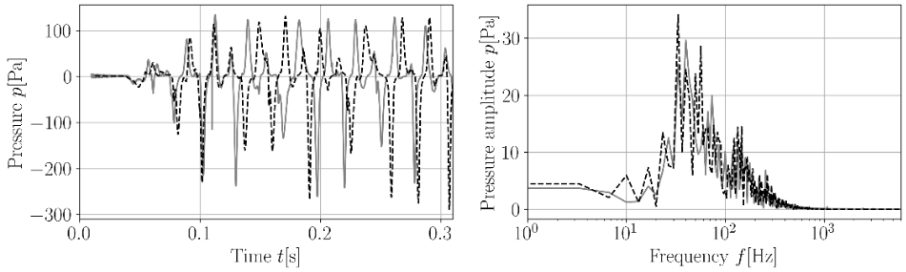

Fig. 7. Pressure values at probe 5 (——— - flexible walls, ----- - rigid walls).

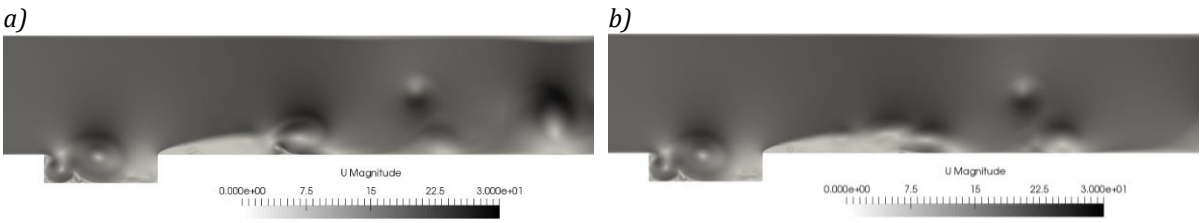

Fig. 8. Velocity distribution inside the duct at t=0.2 s: a) flexible walls, b) rigid walls.

4.2. Vibrations of the cavity walls

In this subsection, the displacement of the probe located at the middle of the bottom cavity wall, both in time and frequency domain is shown. Wall deformations are relatively small but are in line with the estimates resulting from the theory of elasticity for simply supported beams.

The frequencies of vibration partly correspond to the modal frequencies of this structure, especially the first two modes i.e., 190 and 230 Hz. The other frequency components may result from the interactions between the turbulent flow and cavity walls.

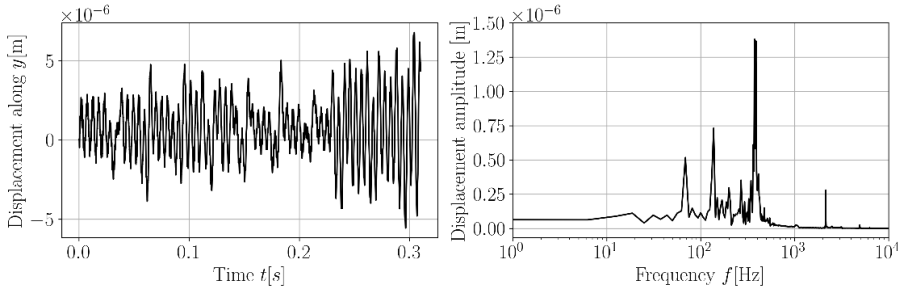

Fig. 9. Displacement of the midpoint of the bottom cavity wall.

4.3. Aeroacoustics results

In this section, the acoustic pressure and sound pressure level obtained at far field with FW-H analogy are presented. The acoustic pressure probes were located at the bottom of the duct, 2 and 5 m downstream of the cavity. The computed pressure is shown in Figs 10 and 11.

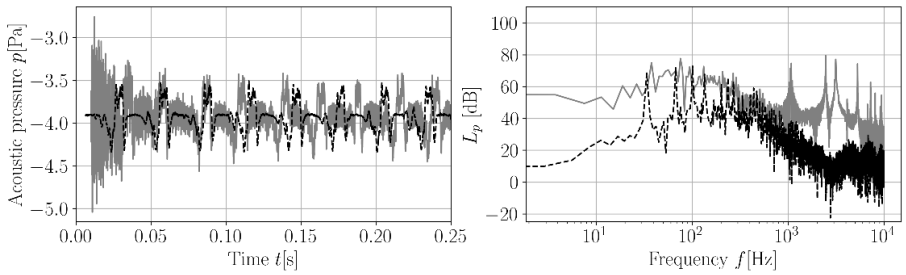

Fig. 10. Acoustic pressure values at acoustic probe 1 (—— - flexible walls, ---- - rigid walls).

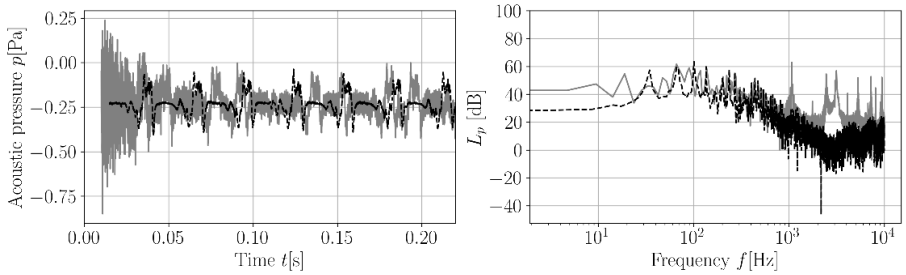

Fig. 11. Acoustic pressure values at acoustic probe 2 (—— - flexible walls, ---- - rigid walls).

In the range of low frequencies, from 10 to 500 Hz, the sound pressure level for both cases is similar, however the type of noise is different. For rigid walls, the tonal noise can be observed, with tone frequencies equal to 35, 65, 100, 150 and 200 Hz. These frequencies correspond to the vortex shedding frequencies, as seen in sect 3.1. For the flexible walls case, the generated noise is broadband in this frequency range.

In the frequency range of 1-10kHz, the cavity with rigid walls is relatively quiet, with SPL within the limits of the numerical error. In this range, the cavity with elastic walls generate tonal noise, with the frequencies equal to 1kHz, 2.5kHz, 3kHz, and higher. These frequencies and tones result from the vibrations of the structure and correspond to the frequencies in this range presented in Fig. 9. Moreover, these frequencies coincide with the higher modal frequencies (8^{th} and 10^{th} modes).

4. Conclusions

In this paper the influence of elastic cavity walls on the flow induced noise was investigated. The numerical analyses of the flow, structural displacement and fluid-structure interactions were conducted with use of appropriate numerical methods – finite volume and finite element methods and corresponding software – OpenFOAM, CalculiX and preCICE.

The results show that not taking elastic walls of the cavity into account can lead to an inexpedient determination of the cavity noise, especially in the higher frequency range. This study is a preliminary analysis of this influence, it is necessary to verify whether in the case of materials with different properties, the higher vibration modes of the structure will have the impact on the generated noise and how significant it will be. It should also be noted that the performed analyses must be verified experimentally.

The obtained results cannot be directly related to the literature due to the fact that, as mentioned in the Introduction, there is no such research and simulation. However, the method itself can be referred to the works of Hron and Turek [16]. The results may be verified on the basis of vibroacoustic simulations decoupled from the flow.

Finally, it must be mentioned that described simulations of fluid-structure interaction are much more computationally expensive. The time of the FSI simulations was ten times longer compared to the CFD simulations not taking flexible walls into account. As for the memory usage, FSI simulations require more memory than CFD, due to additional computational mesh of the FEM method. I t is also worth noting that the disk space is a much bigger problem, because the result files could take up to 1TB for 0.5s of the simulation

Acknowledgments

This research was supported in part by PLGrid Infrastructure.

Additional information

The authors declare no competing financial interests.

References

1. A. Fry. Noise Control in Building Services. Pergamon Press, 1988.
2. I. L. Ver, and L. L. Beranek. Noise and Vibration Control Engineering. Principles and Applications. John Wiley & Sons Ltd., 2006.
3. K. K. Ahuja, J. Mendoza. Effect of Cavity Dimensions, Boundary Layer, and Temperature on Cavity Noise With Emphasis on Benchmark Data to Validate Computational Aeroacoustic Codes. National Aeronautics Space Administration, 1995.
4. M. S. Howe. Edge, cavity and aperture tones at very low Mach numbers. Journal of Fluid Mechanics, 330:61–84, 1997.
5. J. E. Rossiter. Wind-Tunnel Experiments on the Flow over Rectangular Cavities at Subsonic and Transonic Speeds. ARCR & M 3438, 1964
6. S. Weyna. Rozpływ energii akustycznych źródeł rzeczywistych. WNT, 2005.
7. A.I. Alsabery, F. Selimefendigil, I. Hashim, A.J. Chamkha, M. Ghalambaz. Fluid-structure interaction analysis of entropy generation and mixed convection inside a cavity with flexible right wall and heated rotating cylinder. International Journal of Heat and Mass Transfer, 140:331–45, 2019.
8. K. Khanafer. Comparison of Flow and Heat Transfer Characteristics in a Lid-Driven Cavity Between Flexible and Modified Geometry of a Heated Bottom Wall. International Journal of Heat and Mass Transfer, 78:1032–41, 2014.
9. W. A. Sabbar, M. A. Ismael, M. Almudhaffar. Fluid-Structure Interaction of Mixed Convection in a Cavity-Channel Assembly of Flexible Wall. International Journal of Mechanical Sciences, 149:73–83, 2018.
10. H. G. Weller, G. Tabor, H. Jasak, C. Fureby. A tensorial approach to computational continuum mechanics using object-oriented techniques. Computers in Physics, 12(6):620–631, 1998.
11. M. Strelets. Detached eddy simulation of massively separated flows. 39th AIAA Fluid Dynamics Conference and Exhibit, 2001.
12. J. Blazek. Computational Fluid Dynamics. Principles and Applications. Elsevier Ltd. 2015.
13. G. Dhondt, The Finite Element Method for Three-dimensional Thermomechanical Applications. John Wiley & Sons Ltd, 2004.
14. L. Lapidus, G. Pinder. Numerical Solution of Partial Differential Equations in Science and Engineerig. John Wiley & Sons Ltd. 1999.
15. H. J. Bungartz, F. Lindner, B. Gatzhammer, M. Mehl, K. Scheufele, A. Shukaev, B. Uekermann, preCICE – A fully paralel library for multi-physics surface coupling, Computers & Fluids, 141:250-258, 2016.
16. S. Turek, J. Hron. Proposal for Numerical Benchmarking of Fluid–Structure Interaction Between an Elastic Object and Laminar Incompressible Flow. Fluid-Structure Interaction: Modelling, Simulation, Optimisation, 53: 371–85, 2006.
17. J. E. Ffowcs Williams, D. L. Hawkings. Sound Generation by Turbulence and Surfaces in Arbitrary Motion. Philosophical Transactions of the Royal Society of London. Series A, Mathematical and Physical Sciences 264(1151):321–342, 1969.
18. K. S. Brentner, F. Farassat. Modeling aerodynamically generated sound of helicopter rotors. Progress in Aerospace Sciences, 39(2):83–120, 2003.
19. F. Farassat. Derivation of Formulations 1 and 1A of Farassat. NASA/TM-2007-214853. 2007.
20. A. Epikhin, I. Evdokimov, M. Kraposhin, M. Kalugin, S. Strijhak. Development of a Dynamic Library for Computational Aeroacoustics Applications Using the OpenFOAM Open Source Package. Procedia Computer Science. 2015.
21. K. Jarosz, I. Czajka, A. Gołaś. Implementation of Ffowcs Williams and Hawkings aeroacoustic analogy in OpenFOAM, Vibrations in Physical Systems, 27:161–168, 2016.
22. D. Rockwell, E. Naudascher. Review – Self-Sustaining Oscillations of Flow Past Cavities. Journal of Fluids Engineering, 100(2):152–165, 1978.